Supplementary Information

Intermolecular Interaction Mechanism for Ionic Liquids Based on Quaternary Phosphonium Cations with Different Symmetries Using Dielectric and Spectroscopic Analysis

*Mitsuhiro Matsumoto[a], Shoki Nawate[a], Kazuki Takeuchi[a], Yohtaro Inoue[b], Yusuke Tsuchida[c], Katsuhiko Tsunashima[d], and *Hirohisa Yamada[a]*

[a] Department of Chemical Engineering, National Institute of Technology, Nara College, Yamatokoriyama, Nara 639-1080, Japan

[b] Research Division of Polymer Functional Materials, Osaka Research Institute of Industrial Science and Technology, Izumi, Osaka 594-1157, Japan

[c] Department of Integrated Engineering, National Institute of Technology, Yonago College, Yonago, Tottori 683-8502, Japan

[d] Department of Applied Chemistry and Biochemistry, National Institute of Technology, Wakayama College, Gobo, Wakayama 644-0023, Japan

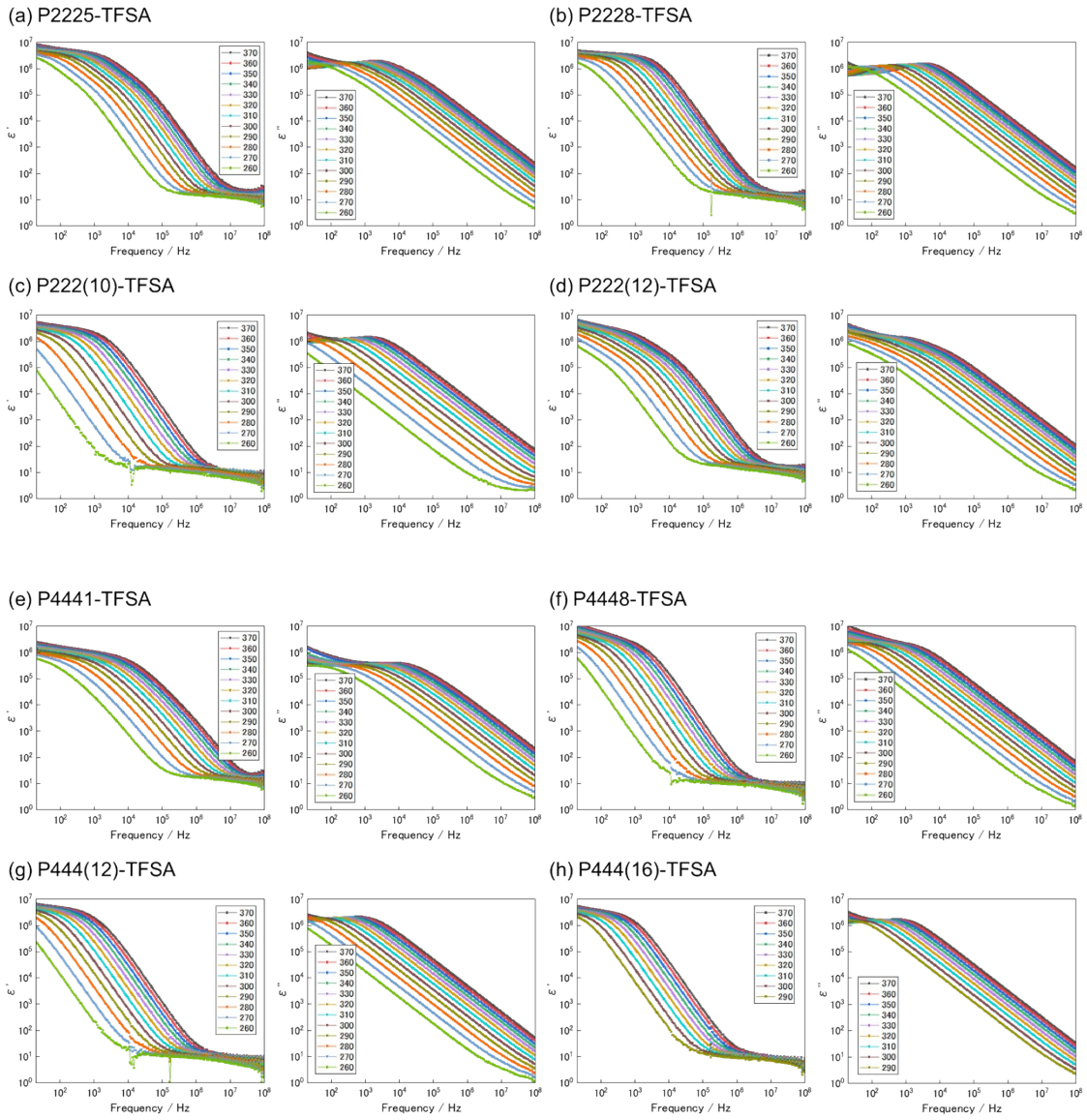

Figure S1. Temperature dependence of the BDS spectra for the TFSA-based P-ILs.

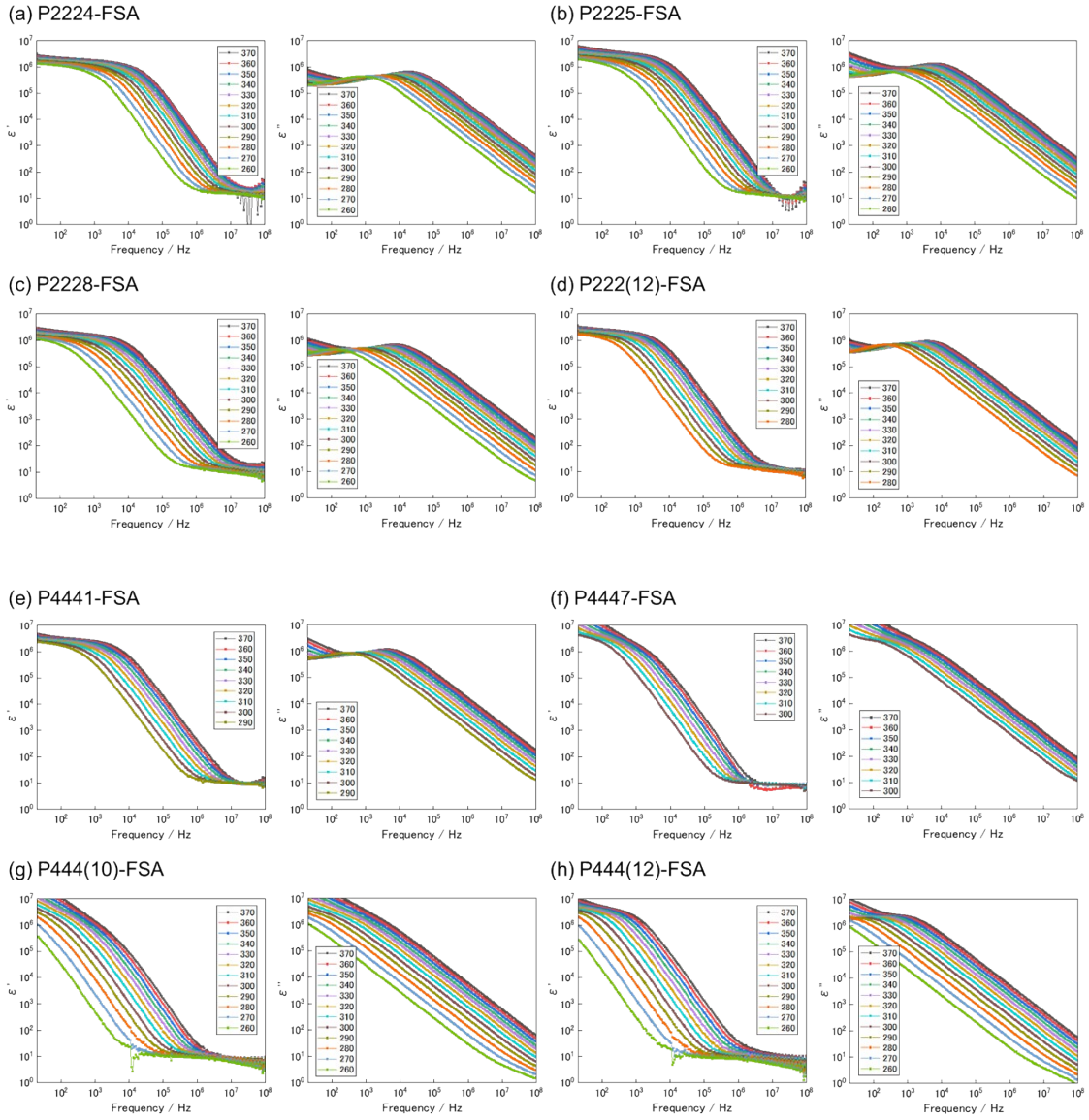

Figure S2. Temperature dependence of the BDS spectra for the FSA-based P-ILs.

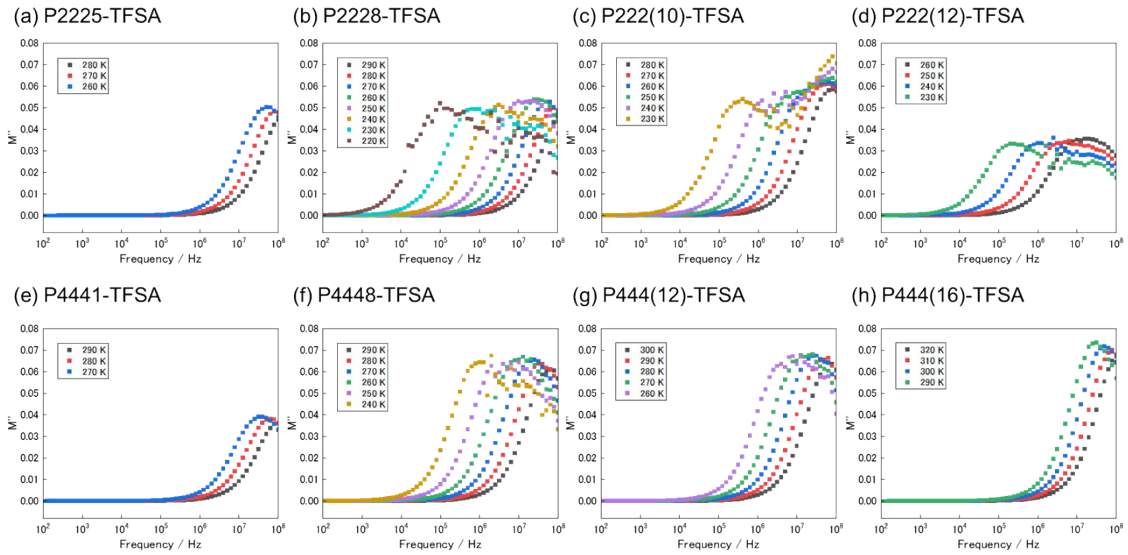

Figure S3. Typical imaginary part of the modulus spectra (M'') for the analysis of dielectric relaxation.

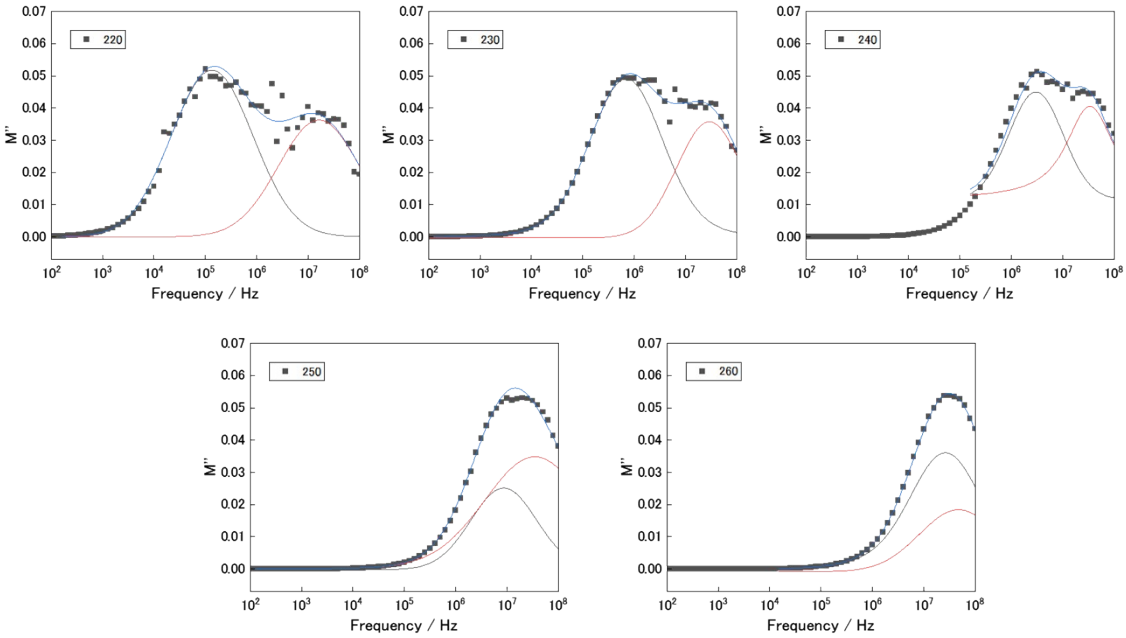

Figure S4. Spectral decomposition results of M'' spectra for P2228-TFSA.

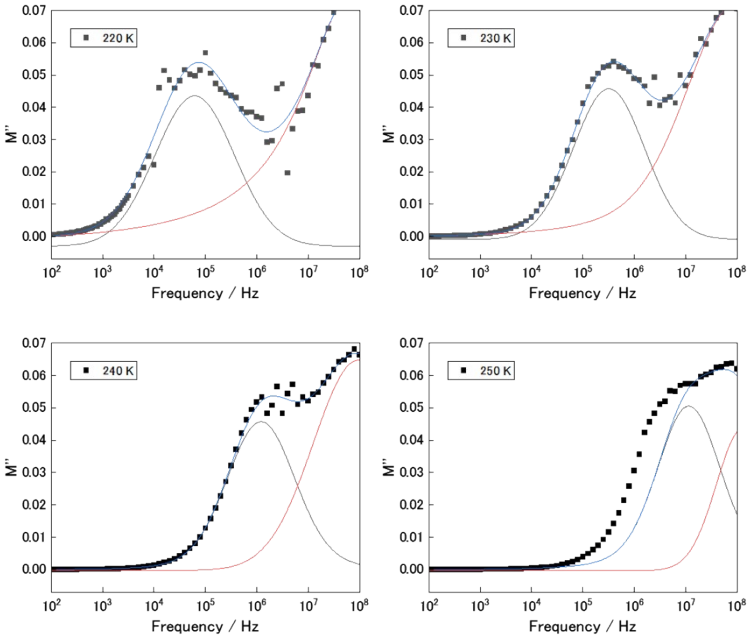

Figure S5. Spectral decomposition results of M'' spectra for P222(10)-TFSA.

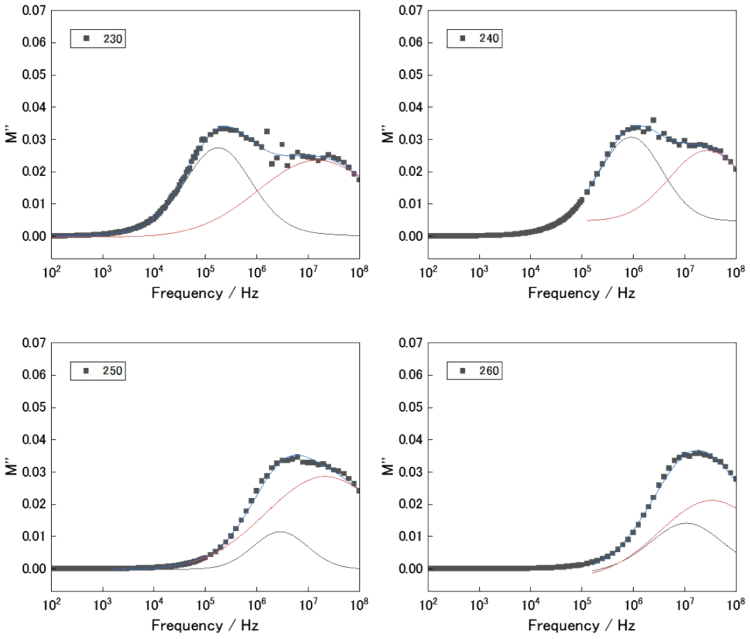

Figure S6. Spectral decomposition results of M'' spectra for P222(12)-TFSA.

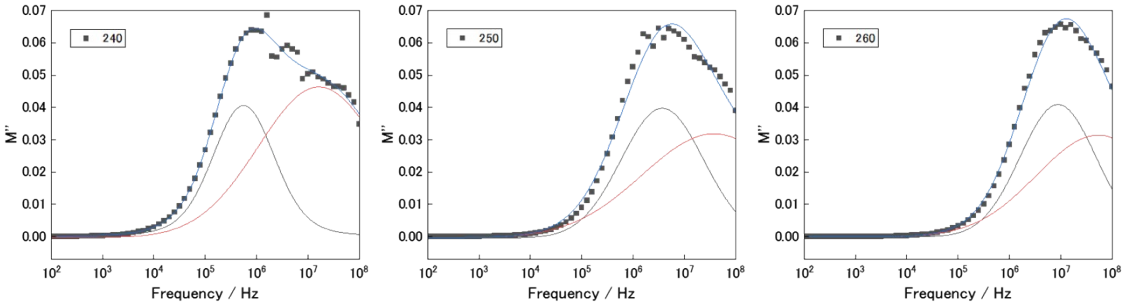

Figure S7. Spectral decomposition results of M'' spectra for P4448-TFSA.

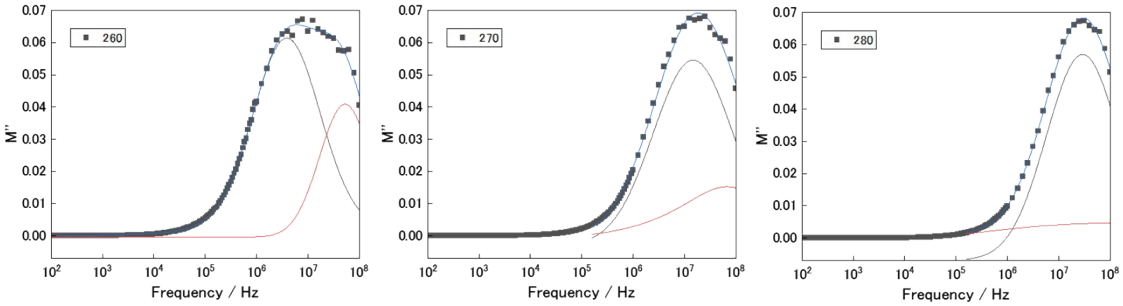

Figure S8. Spectral decomposition results of M'' spectra for P444(12)-TFSA.

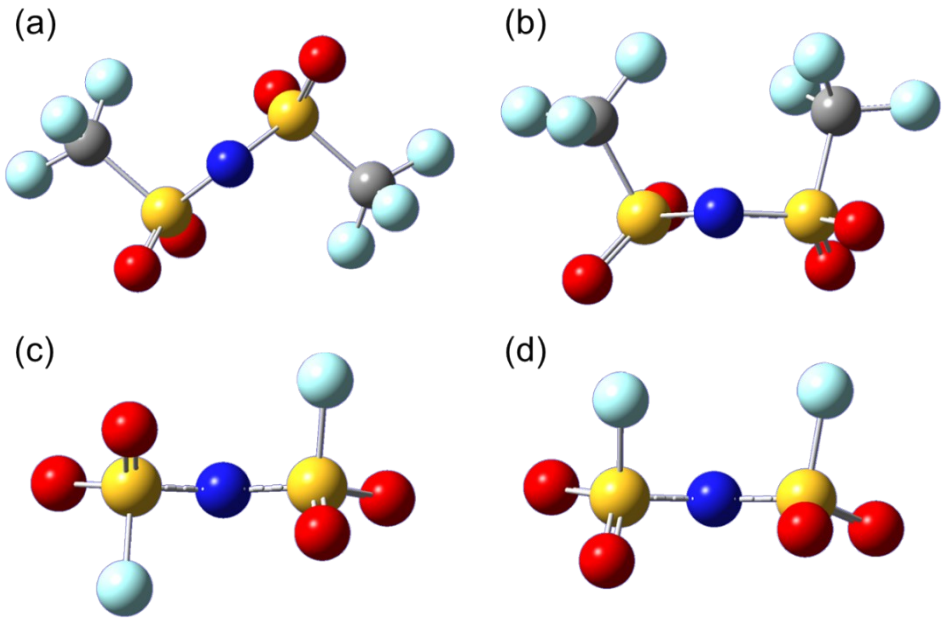

Figure S9. Optimized geometry structures obtained by DFT calculations. The obtained dipole moments are as follows: (a) Transoid-TFSA = 0.45 D, (b) Cisoid-TFSA = 4.86 D, (c) Transoid-FSA = 0.20 D, and (d) Cisoid-FSA = 0.78 D. The following table is a summary of gaussian thermochemistry.

	TFSA		FSA		Unit
	Trans (C2)	Cis (C1)	Trans (C2)	Cis (C1)	
Electronic Energy (EE)	-1826.6686	-1826.6674	-1351.2841	-1351.2826	Hartree
Zero-point Energy Correction	0.053994	0.053992	0.029654	0.029611	Hartree
Thermal Correction to Energy	0.068238	0.068225	0.038013	0.038009	Hartree
Thermal Correction to Enthalpy	0.069183	0.069169	0.038957	0.038954	Hartree
Thermal Correction to Free Energy	0.010394	0.010816	-0.004363	-0.005475	Hartree
EE + Zero-point Energy	-1826.6146	-1826.6134	-1351.2544	-1351.253	Hartree
EE + Thermal Energy Correction	-1826.6004	-1826.5992	-1351.2461	-1351.2446	Hartree
EE + Thermal Enthalpy Correction	-1826.5994	-1826.5982	-1351.2451	-1351.2436	Hartree
EE + Thermal Free Energy Correction	-1826.6582	-1826.6566	-1351.2885	-1351.2881	Hartree
E (Thermal)	42.82	42.812	23.853	23.851	kcal/mol
Heat Capacity (Cv)	49.383	49.419	28.921	28.952	cal/mol-kelvin
Entropy (S)	123.73	122.814	91.175	93.509	cal/mol-kelvin
Dipole moment	0.45	4.86	0.20	0.78	debye

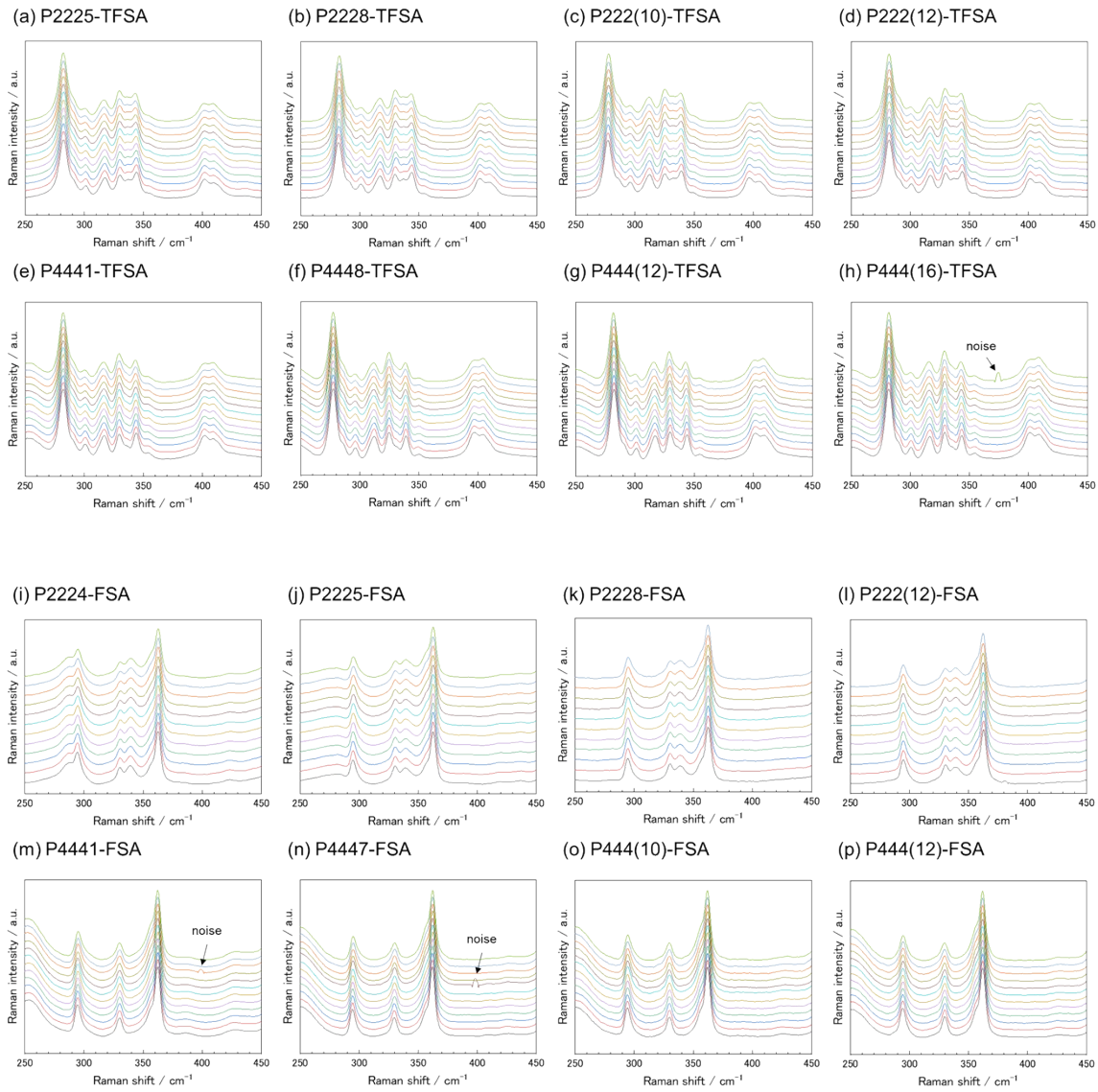

Figure S10. Temperature dependence of the Raman spectra for the P-ILs.

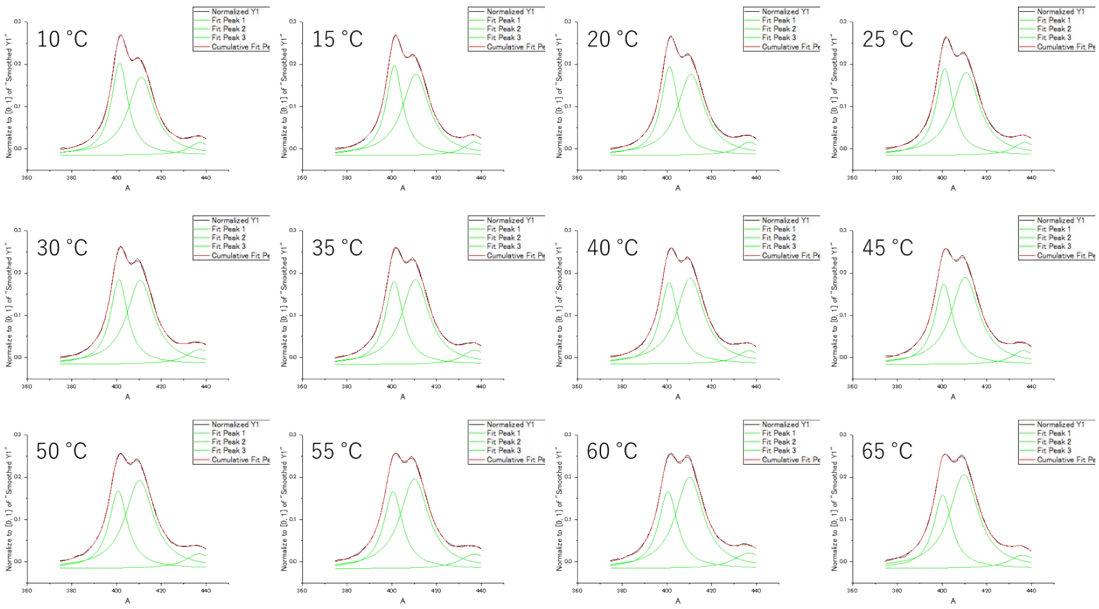

Figure S11. Spectral decomposition results of Raman spectra for P2225-TFSA. The set temperature before correction is displayed in each graph.

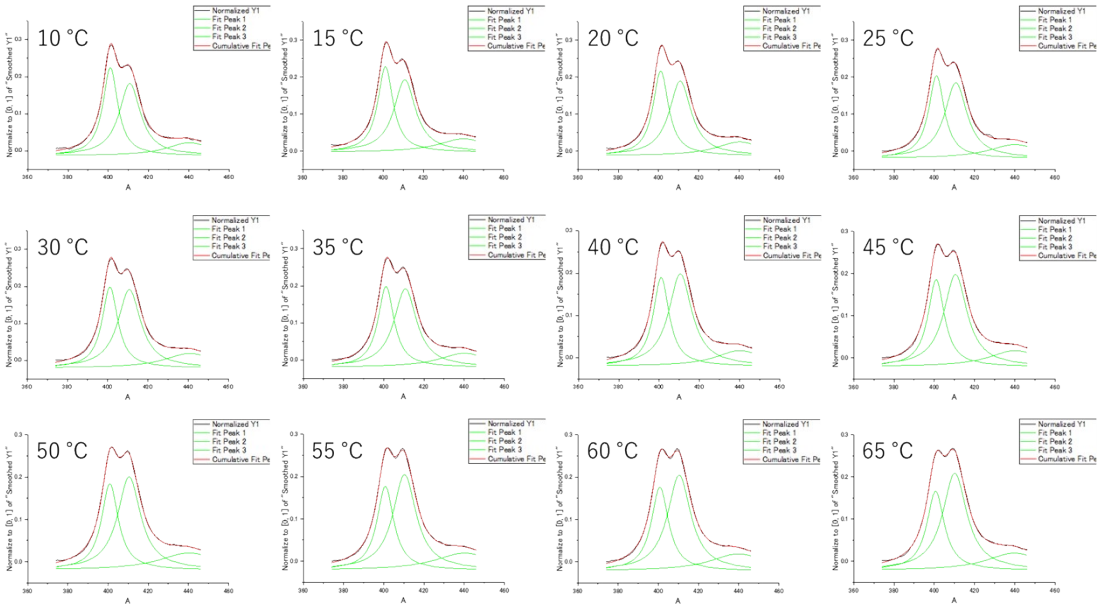

Figure S12. Spectral decomposition results of Raman spectra for P2228-TFSA. The set temperature before correction is displayed in each graph.

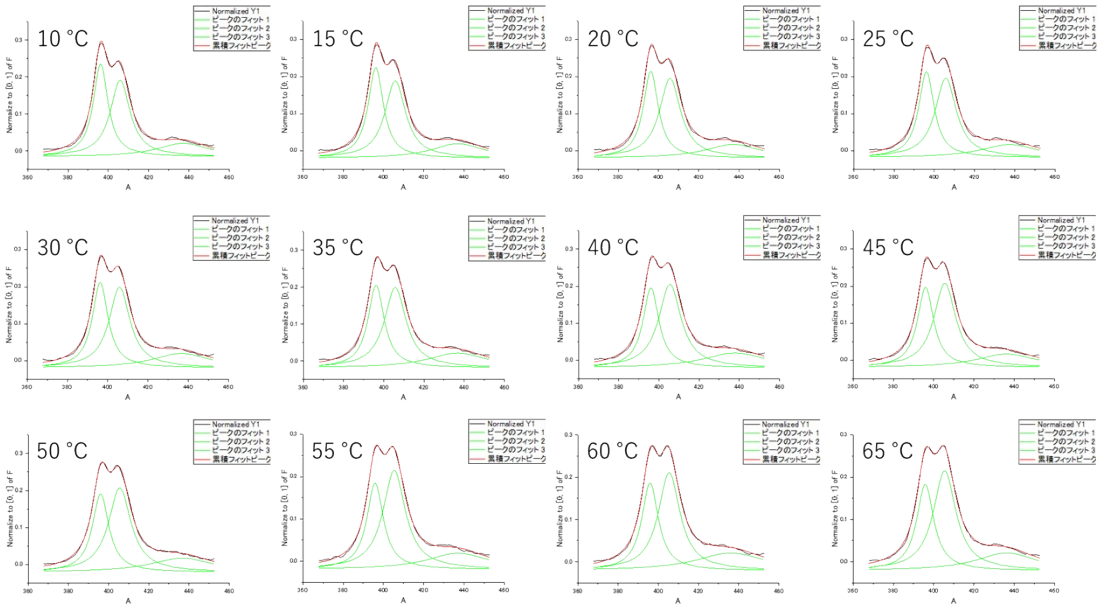

Figure S13. Spectral decomposition results of Raman spectra for P222(10)-TFSA. The set temperature before correction is displayed in each graph.

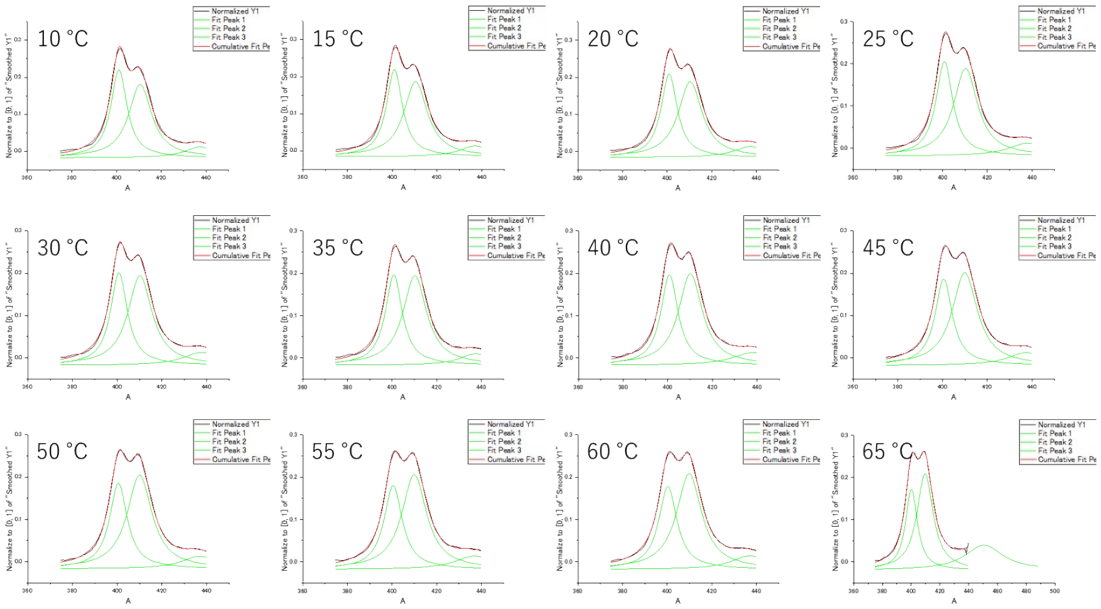

Figure S14. Spectral decomposition results of Raman spectra for P222(12)-TFSA. The set temperature before correction is displayed in each graph.

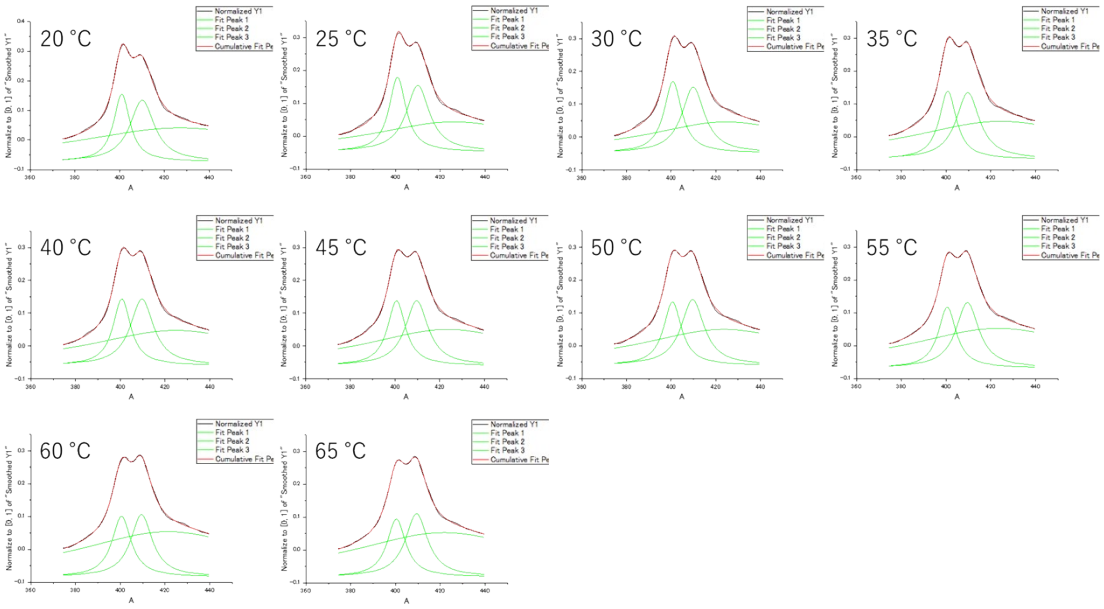

Figure S15. Spectral decomposition results of Raman spectra for P4441-TFSA. The set temperature before correction is displayed in each graph.

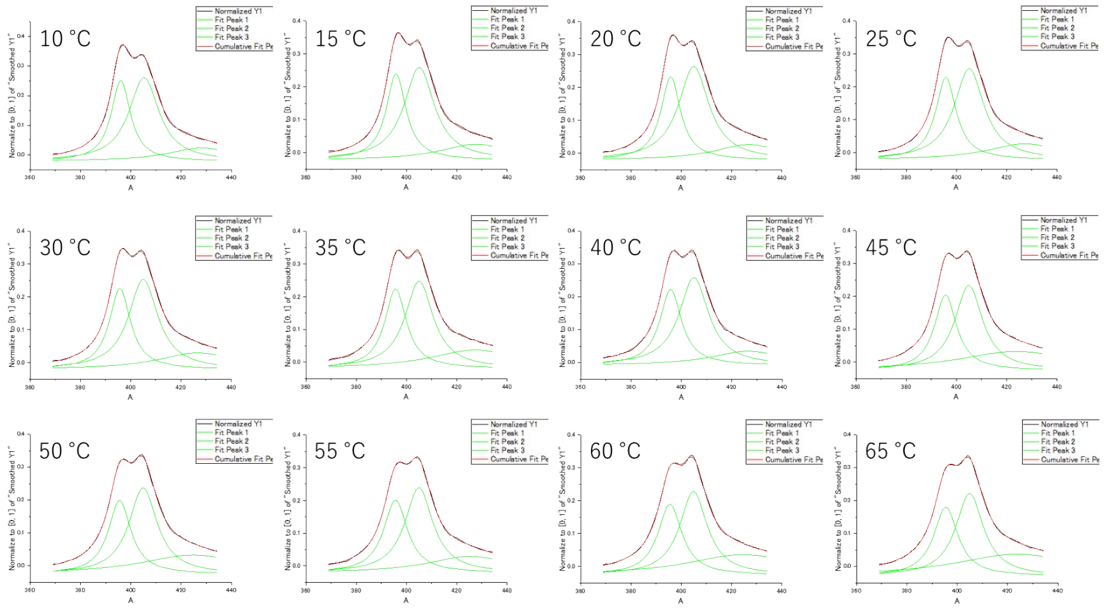

Figure S16. Spectral decomposition results of Raman spectra for P4448-TFSA. The set temperature before correction is displayed in each graph.

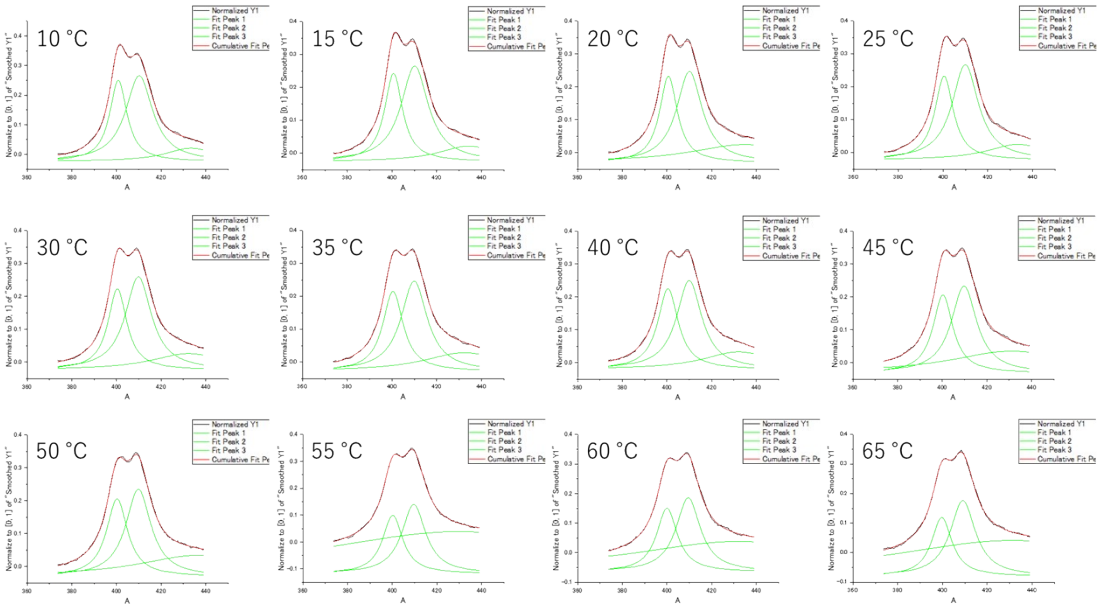

Figure S17. Spectral decomposition results of Raman spectra for P444(12)-TFSA. The set temperature before correction is displayed in each graph.

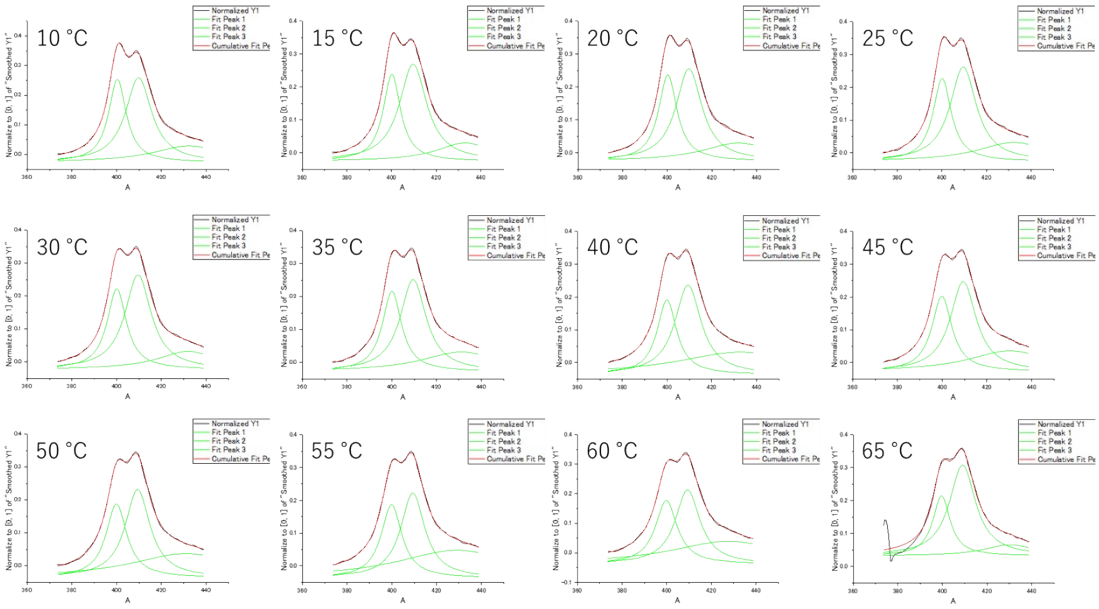

Figure S18. Spectral decomposition results of Raman spectra for P444(16)-TFSA. The set temperature before correction is displayed in each graph.

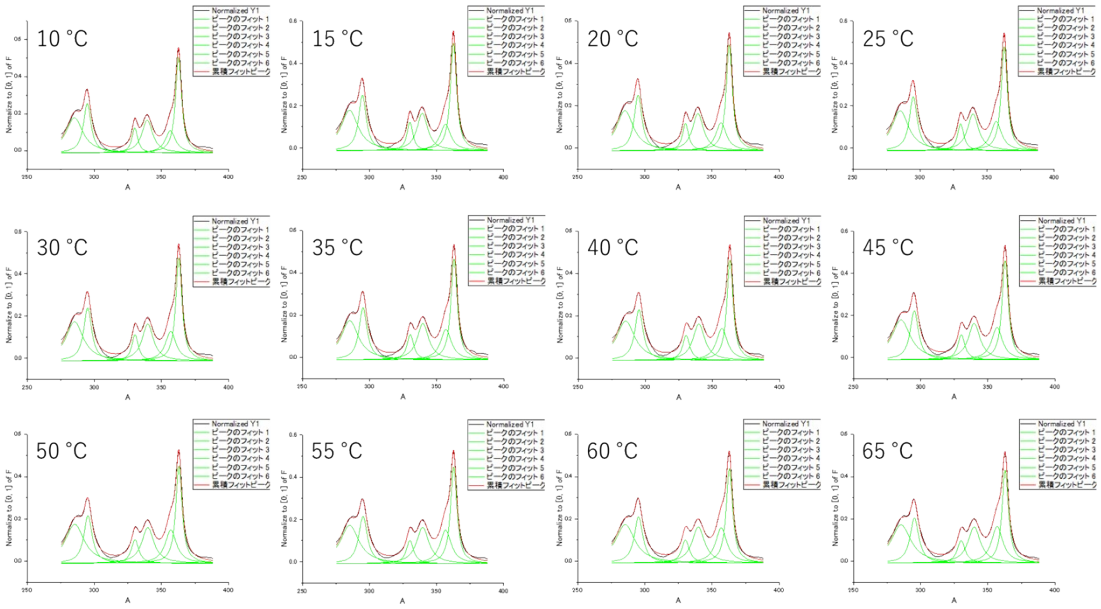

Figure S19. Spectral decomposition results of Raman spectra for P2224-FSA. The set temperature before correction is displayed in each graph.

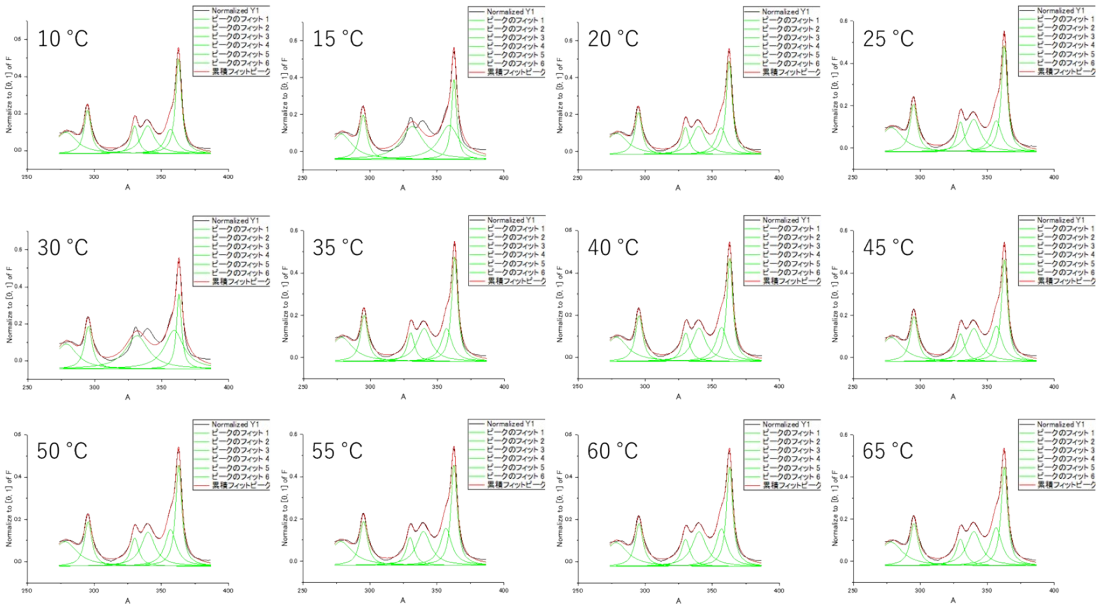

Figure S20. Spectral decomposition results of Raman spectra for P2225-FSA. The set temperature before correction is displayed in each graph.

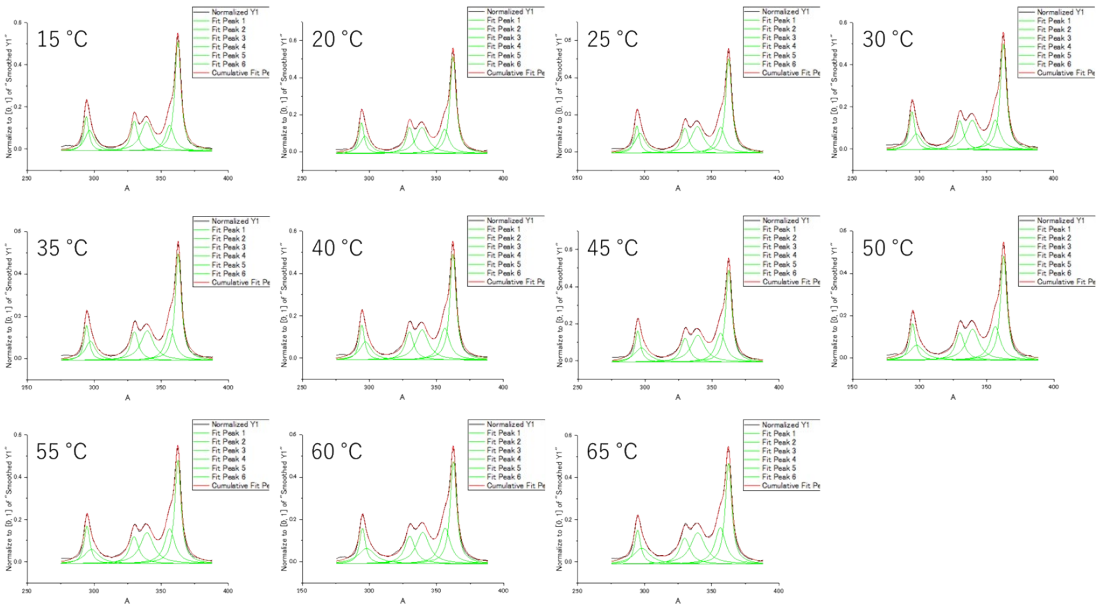

Figure S21. Spectral decomposition results of Raman spectra for P2228-FSA. The set temperature before correction is displayed in each graph.

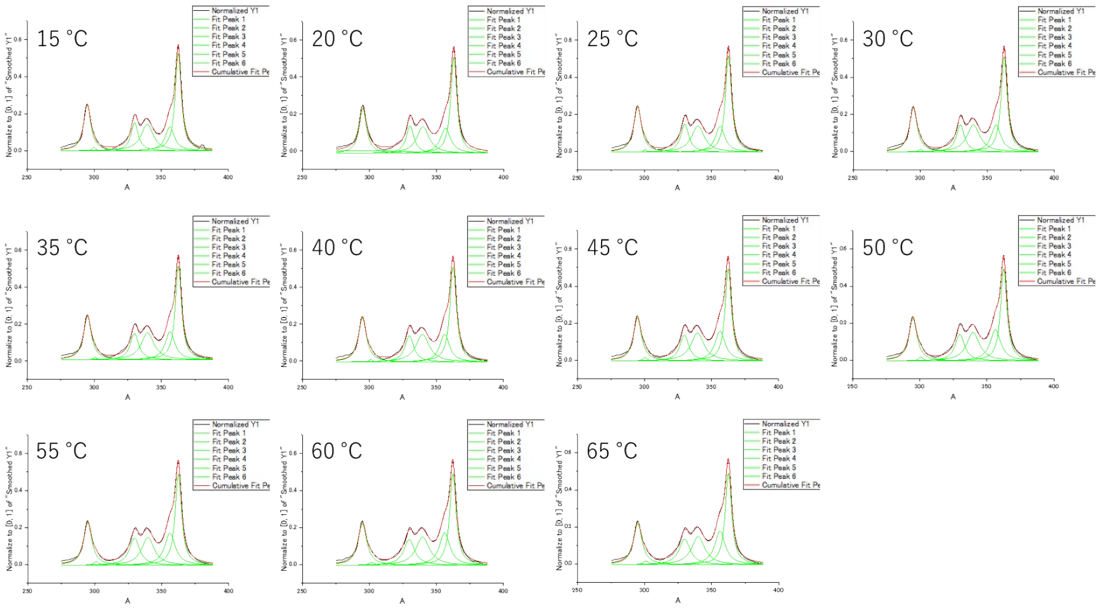

Figure S22. Spectral decomposition results of Raman spectra for P222(12)-FSA. The set temperature before correction is displayed in each graph.

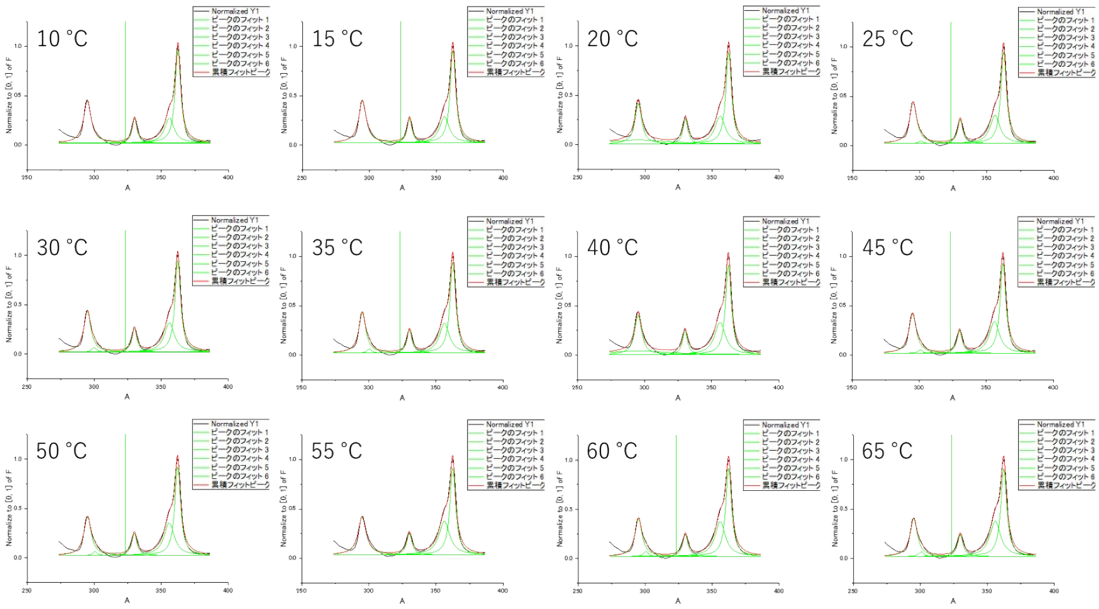

Figure S23. Spectral decomposition results of Raman spectra for P4441-FSA. The set temperature before correction is displayed in each graph.

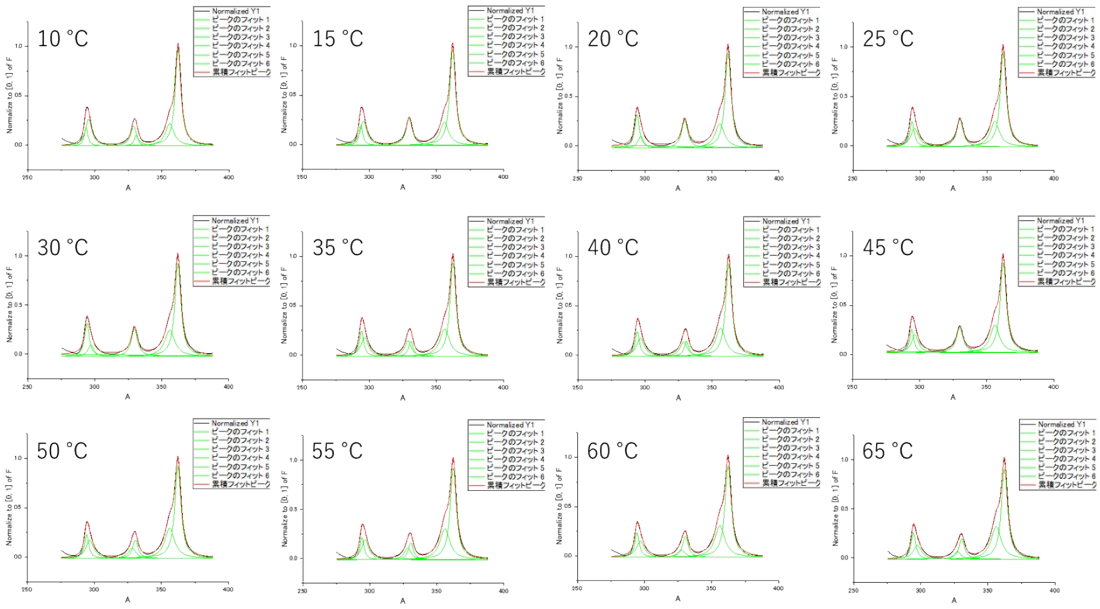

Figure S24. Spectral decomposition results of Raman spectra for P4447-FSA. The set temperature before correction is displayed in each graph.

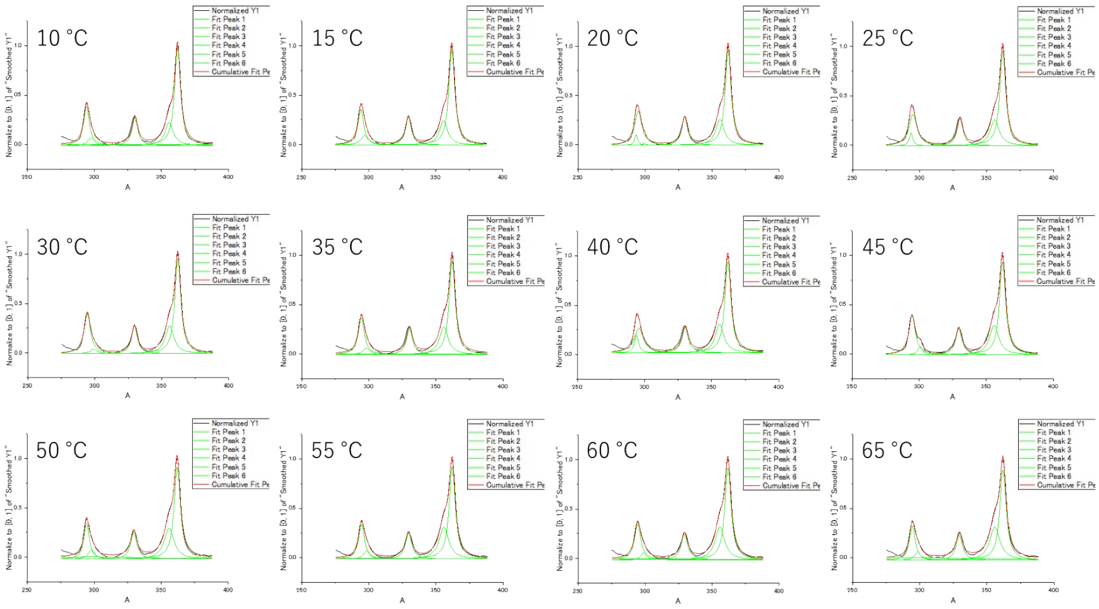

Figure S25. Spectral decomposition results of Raman spectra for P444(10)-FSA. The set temperature before correction is displayed in each graph.

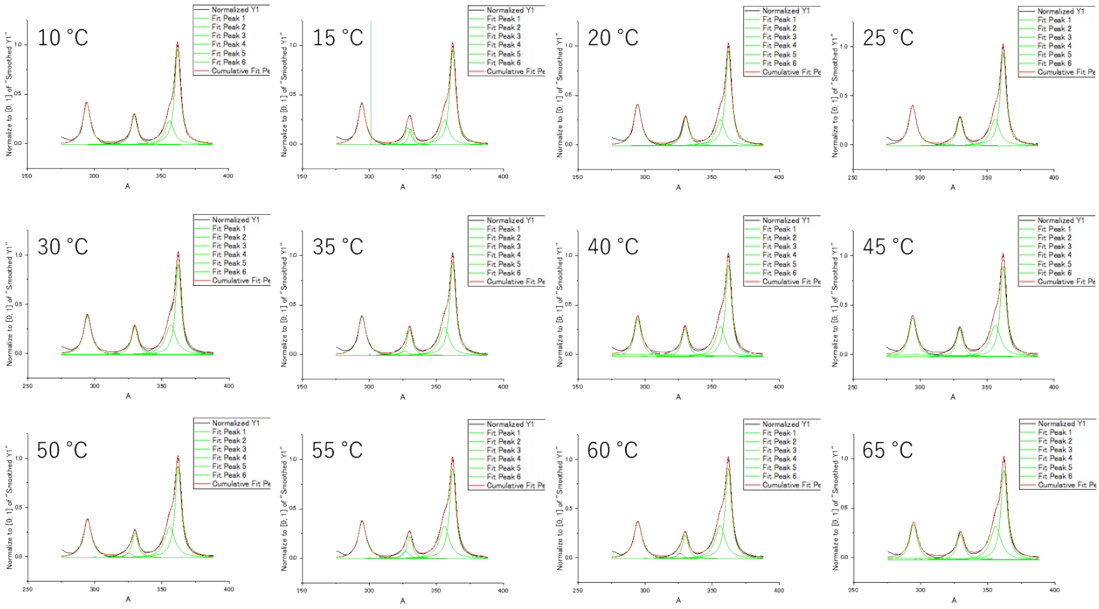

Figure S26. Spectral decomposition results of Raman spectra for P444(12)-FSA. The set temperature before correction is displayed in each graph.

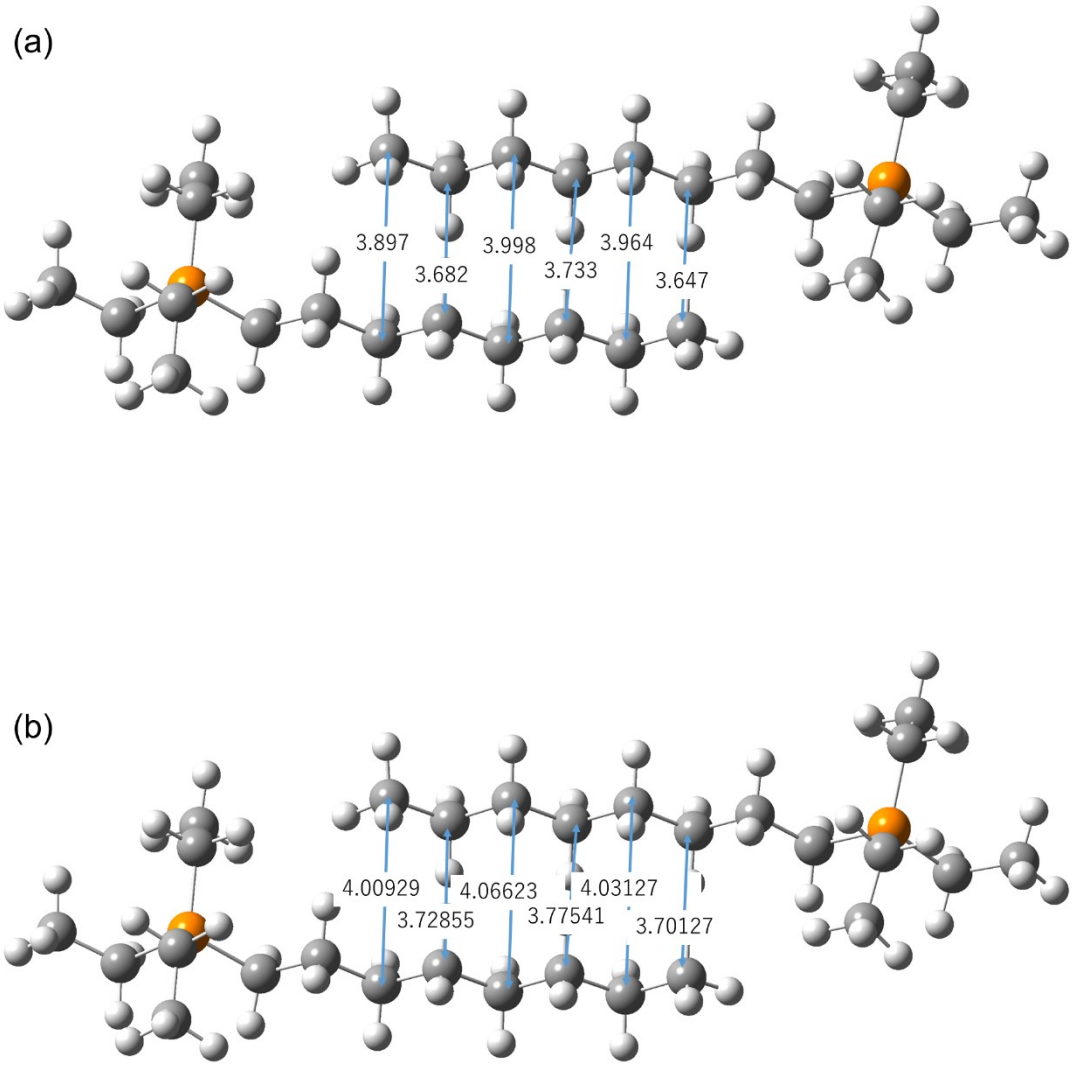

Figure S27. Optimized geometry structures of a P2228 dimer obtained by DFT calculations. The ωB97XD/6-31G** and APFD/6-31G** levels of theory were used for (a) geometry optimization and (b) subsequent single point energy calculation, respectively. In (b), the BSSE-corrected energy gap for $2[P_{2228}]^{+} \rightarrow [(P_{2228})_2]^{2+}$ was determined to be +13.8 kcal/mol, which indicates that the dimer structure of the P222R cations is locally stable (no imaginary frequencies were obtained).